Photon Factory Activity Report 2001 #19B
–Users' Report–

10A/1999G019

Compression of O-H- -O distances of Phase A, $Mg_7Si_2H_6O_{14}$

Yasuhiro KUDOH*[1], Takahiro KURIBAYASHI[1], Hiroyuki KAGI[2], Satoshi SASAKI[3] and Masahiko TANAKA[4]
[1]Tohoku University., Sendai 980-8578, Japan
[2]University of Tokyo, Tokyo 113-0033, Japan
[3]Tokyo Institute of Technology Nagatuda, Yokohama 226-8503, Japan
[4]KEK-PF, Tukuba, 305-0801, Japan

Sets of X-ray diffraction intensities up to $\sin\theta/\lambda$ = 0.7~1.0 $Å^{-1}$ were measured with a 60×50×30 μm single crystal of phase A, $Mg_7Si_2H_6O_{14}$ synthesized by Kagi et al. (2000)[1] using a multi-anvil apparatus at conditions of 1000℃ and 10 GPa. X-ray diffraction data at ambient pressure were measured with MoKα radiation (50 kV, 40 mA). X-ray diffraction data at high pressures were measured using synchrotron radiation of wave lengths 0.6965 Å, 0.6993 Å and 0.7026 Å at 4.5 GPa, 9.1 GPa and 9.4 GPa, respectively at the beam line BL-10A, Photon Factory, Tukuba, Japan. Result of electron microprobe analysis yields a chemical composition of $Mg_{6.99}Si_{1.99}H_{6.06}O_{14}$. The difference of the total weight was ascribed to H_2O. The modified Merrill-Bassett type diamond anvil pressure cell [2] was used. A 0.25 mm thick stainless steel (SUS301) plate was used as gasket material. As a fluid pressure medium, a 4:1 mixture of methanol and ethanol was used. The pressure was calibrated using the ruby fluorescence method. The unit cell parameters obtained using 15~24 reflections with 2θ from 10° to 50° are given in Table 1. Out of 2300 reflections in a sphere which were accessible with diamond anvil high pressure cell, a total of 164~299 symmetry independent reflections (Io≥1.5σIo ~ Io≥3σIo) were obtained by averaging the symmetry equivalent intensities in Laue group 6/m. Intensities were corrected for Lorentz factor and no absorption correction was applied because of the sufficiently small value of μr (<0.04). From the study of neutron powder diffraction data of phase A at ambient pressure and 3.2 GPa, Kagi et al. (2000)[1] reported that increased pressure further increases the hydrogen bonding of D1 compared to D2 and O4-D2---O3 showed no significant increase or decrease in hydrogen bonding in the pressure range investigared. Our results in the present study are in general agreement with the observation of Kagi et al. (2000)[1]. The O-O distances around hydrogen atoms in Table 2 indicate that both O2-O3 and O4-O3 distances significantly decrease and O2-O3 distance decrease more than O4-O3 distance with increasing pressure. O2-O3 distance decrease around 10% at 9.4 GPa, while O4-O3 distance decrease around 6% at the same pressure. It should be noted that the trend of O4-O3 is on a line of the O-O decrease in brucite up to 9.3 GPa reported by Parise et al. (1994) [3].

Table 1. Unit cell parameters, number of Fo and R values

P(GPa)	0	4.5	9.1	9.4
a (Å)	7.8604(7)	7.756(1)	7.6445(3)	7.644(1)
c (Å)	9.5702(8)	9.469(3)	9.383(7)	9.371(2)
$2\theta_{max}$(°)	60.0	90.0	60.0	80.0
Radiation	MoKα	Synchrotron		
#of Fo	363	299	164	255
	Io≥σ3Io	Io≥σ3Io	Io≥σ1.5Io	Io≥σ3Io
R(%)	5.0	9.6	7.4	7.9
Rw(%)	6.0	9.1	8.4	7.3

Table 2. Atomic parameters of O2, O3 and O4 (parameters of all other atoms are not listed)

P(GPa)	0.0	4.5	9.1	9.4
O2 x	0.4759(8)	0.4728(15)	0.4748(13)	0.4700(12)
y	0.0983(8)	0.0985(15)	0.1046(13)	0.0985(12)
z	0.4853(8)	0.4848(20)	0.4836(22)	0.4815(20)
B	0.17(8)	0.4(1)	0.0(2)	0.0(1)
O3 x	0.4510(7)	0.4500(11)	0.4475(10)	0.4486(10)
y	0.2927(7)	0.2891(11)	0.2827(10)	0.2873(11)
z	0.2334(8)	0.2421(29)	0.2472(24)	0.2517(30)
B	0.13(9)	0.0(1)	0.0(2)	0.5(1)
O4 x	0.1660(7)	0.1634(10)	0.1539(11)	0.1604(9)
y	0.4344(7)	0.4344(11)	0.4310(11)	0.4370(10)
z	0.2406(8)	0.2443(27)	0.2628(29)	0.2549(25)
B	0.24(9)	0.0(1)	0.0(2)	0.0(1)

Table 3. O-O distances (Å) around H

P(GPa)	0	4.5	9.1	9.4
O2-H--O3	2.91(1)	2.79(3)	2.66(3)	2.64(2)
O4-H--O3	3.168(9)	3.06(2)	2.92(1)	2.99(1)

References

[1] H. Kagi, J.B. Parise, H. Cho, G.R. Rossman, J.S. Loveday, *Phys. Chem. Minerals*, **27** , 225 (2000)
[2] Y. Kudoh, H. Takeda, *Physica* **139&140** B, 333, (1986)
[3] J. B. Parise, K. Leinenweber, D. J. Weidner, K. Tan, R. B. Von Dreele, Am. Min., **79**, 193 (1994)

*ykudoh@mail.cc.tohoku.ac.jp

18C/1999G225

High pressure phase III of tellurium

Masaharu TAKUMI*[1], Takeshi MASAMITSU[1] and Kiyofumi NAGATA[1, 2]
[1]Dept. of Appl. Phys., Fukuoka Univ., Fukuoka 814-0180, Japan
[2]Advanced Materials Institute, Fukuoka Univ., Fukuoka 814-0180, Japan

Introduction

Selenium (Se) and tellurium (Te) at ambient condition have trigonal form which consists of 3_1 helix chain molecules. With increasing pressure, both Se and Te change from the molecular crystal, through several high-pressure phases, to bcc metallic phase.[1], [2] In the process of this pressure-induced molecular dissociation, inter- and intramolecular chemical bonding-characters are expected to change with pressure. In order to discuss the pressure dependence of the bonding character in detail, it is necessary to obtain the electron density distribution of Se and Te at various pressures by maximum entropy method (MEM). Since the structure of the high pressure phases of Te-III is ambiguous,[3] however, the correct structure of Te-III has been obtained before the X-ray structural analysis by the MEM.

Experimental

The powdered samples of commercial tellurium with 99.999% purity were loaded into a diamond-anvil high-pressure cell. Methanol : ethanol : water mixture in 16 : 3 : 1 ratio was used as pressure-transmitting medium. Incident X-ray beam was monochromatized to a wavelength of 0.6200 Å at BL-18C. X-ray diffraction patterns were analyzed using Rietveld refinement program RIETAN-94.[4]

Results and Discussion

Previously reported phase transitions from Te-I to Te-II, and from Te-II to Te-III are observed at 4 GPa and 7 GPa, respectively.[1], [5] The phase transition from Te-III to Te-IV is observed at 28 GPa. This phase transition is clarified to be of second order, because the X-ray diffraction pattern changes continuously with pressure at pressure between 7 GPa and 32 GPa where the next phase transition from Te-IV to Te-V occurs.

To determine the structure of Te-III, Rietveld analyses were performed using many kinds of unit cells and space groups which were derived from rhombohedral Te-IV lattice. Minimum reliability factor is obtained for a monoclinic lattice whose space group is $C2/m$. The reliability factor (R_{wp}) is less than 15 % for all Rietveld analyses of the high pressure phase at pressure between 7 GPa and 28 GPa. The obtained structure parameters at 10.4 GPa are as follows.

a=8.3790(14) Å,	b=4.7300(8) Å,	c=3.8710(7) Å,
β=88.63(1) °,	V=153.38 Å^3,	Z=6,
x_1=0 (fixed),	y_1=0 (fixed),	z_1=0 (fixed),
x_2=0.328(8),	y_2=0 (fixed),	z_3=0.673(21).

The structure of Te-III is shown in Fig. 1. Solid lines represent the short bonds of about 3 Å. This zigzag layer structure is different from those obtained for tellurium and selenium previously.[5], [6]

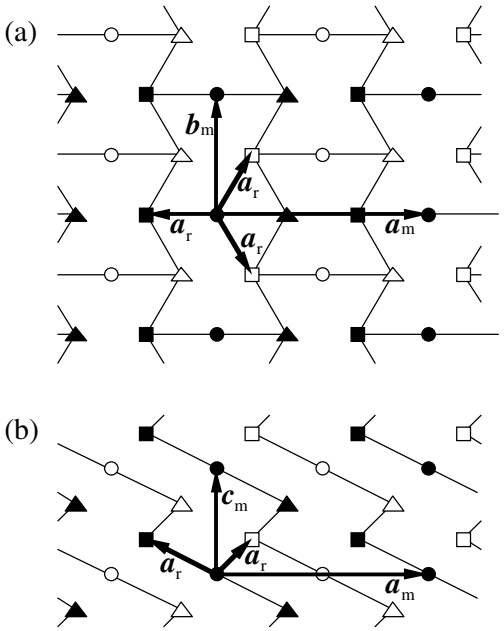

Figure 1. The structure of Te-III phase viewed along the c-axis (a) and the b-axis (b). Solid lines show the short bonds of about 3.0 Å. The symbols $\boldsymbol{a}_m$, $\boldsymbol{b}_m$ and $\boldsymbol{c}_m$ represent the lattice vectors of Te-III monoclinic phase. The symbol $\boldsymbol{a}_r$ represents the lattice vector of Te-IV rhombohedral phase.

References

[1] G. Parthasarathy and W. B. Holzapfel, Phys. Rev. **B37**, 8499 (1988).
[2] Y. Akahama, M. Kobayashi and H. Kawamura, Phys. Rev. **B56**, 5027 (1997).
[3] Y. Akahama and H. Kawamura, Rev. High Pressure Sci. and Technol., **5**, 143 (1996). Y. Akahama, M. Kobayashi and H. Kawamura, Phys. Rev. **B47**, 20 (1993).
[4] Y. -I. Kim and F. Izumi, J. Ceram. Soc. Jpn. **102**, 401 (1994).
[5] K. Aoki, O. Shimomura and S. Minomura, J. Phys. Soc. Jpn. **48**, 551 (1980).
[6] Y. Ohmasa, I. Yamamoto, M. Yao and H. Endo, J. Phys. Soc. Jpn., **64**, 4766 (1995).

* takumi@fukuoka-u.ac.jp

14C2, AR-NE5C/2000G044

Structure of liquid InSb under pressure

Takanori HATTORI, Naohito TAGA, Yukinobu TAKASUGI, Tomohiro KINOSHITA, Kazuhiko TSUJI*
Keio Univ., Hiyoshi, Kohoku-ku, Yokohama 223-8522, Japan

Introduction

In order to elucidate the effects of the ionicity in chemical bonding on the structure of covalent liquids, we have investigated the structure of liquid III-V compounds. Recently we reported the structure of liquid GaSb [1] under pressure, which is relatively less ionic among III-V compounds. Succeeding to the study, we have investigated the structure of liquid InSb, which is more ionic than liquid GaSb, at pressures up to 6.7 GPa.

Experimental

X-ray diffraction patterns were taken by an energy-dispersive method using the synchrotron radiation source and the multi-anvil high-pressure apparatus. The pressure and temperature conditions of the measurements are shown in Fig. 1, together with the previously reported phase diagram [2,3]. The data were taken by MAXIII and MAX80 installed at BL-14C2 and AR-NE5C, respectively.

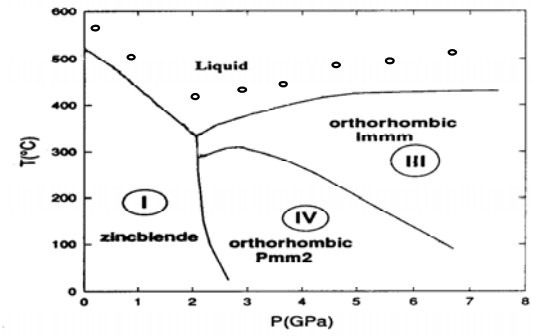

Fig.1 PT conditions for the data collection.

Results and Discussion

The structure factors, S(Q), at high pressures are shown in Fig. 2. The presence of the shoulder at the right-side of the first peak implies a non-simple local structure in the liquid. With increasing pressure, the first and second peaks shift toward lower and higher Q values, respectively. It shows that, in a microscopic scale, the local structure of liquid InSb does not contract uniformly, but changes anisotropically with increasing pressure.

The pair distribution functions, g(r), at high pressures are shown in Fig. 3. The position of the first peak is almost constant with increasing pressure in spite of the volume contraction. On the other hand, the positions of the hump and the second peaks shift markedly with pressure. From the analysis of g(r) on the basis of a quasi-crystalline model, it is suggested that the local structure of liquid InSb consists of the mixture of the beta-tin-like and the body-centred cubic (bcc)-like structures. The fractional ratio of bcc was found to increase with pressure. Corresponding to this view, the coordination number of liquid InSb increases from about 5.8 to 7.5. These results shows that liquid InSb contacts by changing its local structure from the low coordinated beta-tin-like structure to the high-coordinated bcc-like one under pressure. The pressure-induced change in the local structures is almost the same as that in liquid GaSb. In spite of the difference of ionicity in chemical bonding between InSb and GaSb, no remarkable differences were observed in their local structures and the pressure dependence.

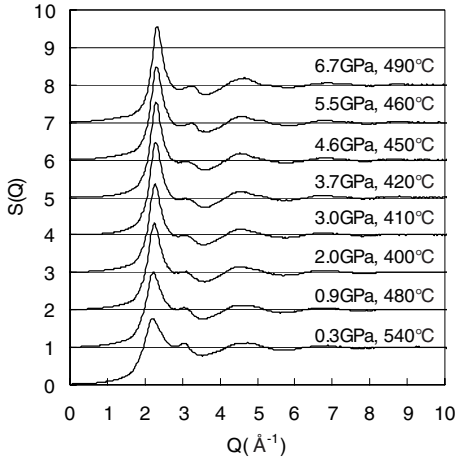

Fig. 2 S(Q) of liquid InSb at high pressures.

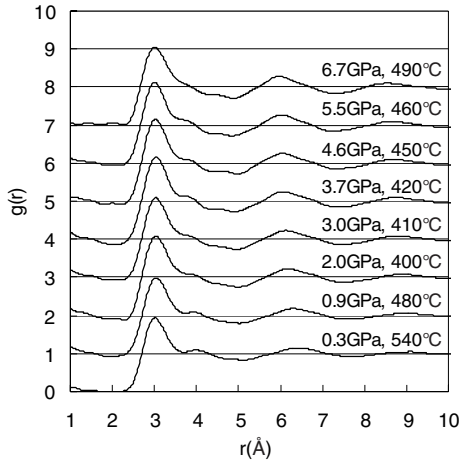

Fig. 3 g(r) of liquid InSb at high pressures.

References

[1] T. Hattori et al., J. Phys. Condens. Matter, (in press).
[2] R. J. Nelmes et al., Phys. Rev. B **47**, 35 (1993).
[3] M. I. McMahon and R. J. Nelmes, phys. stat. sol. (b) **198**, 389 (1996)
* tsuji@phys.keio.ac.jp

14C2/2000G211

Kinetics of decomposition reaction in pyrope $Mg_3Al_2Si_3O_{12}$

Tomoaki KUBO[1*], Eiji OHTANI[1], Tadashi KONDO[1], Takumi KATO[2], Motomasa TOMA[1], Takumi KIKEGAWA[3]
[1]Tohoku Univ., Sendai, Miyagi 980-8578, Japan
[2]Univ. Tsukuba, Ibaraki 305-8571, Japan
[3]KEK-PF, Tsukuba, Ibaraki 305-0801, Japan

Introduction

The subducted oceanic lithosphere is mainly composed of basaltic crust and the underlying peridotite layer, in which garnet and silicate spinel are the major constituent minerals, respectively, at the depth of ~500-600 km. As the slab descends into the lower mantle, garnet and spinel decompose to perovskite plus aluminous phase (post-garnet transformation) and perovskite plus ferro-periclase (post-spinel transformation), respectively. Metastability in these transformations under subduction zone conditions greatly affect on dynamics of the slab in the deep mantle. Mechanisms and kinetics of the post-spinel transformation has been examined before [1]. Here we report results of the post-garnet transformation kinetics in pyrope $Mg_3Al_2Si_3O_{12}$. We performed high-pressure *in-situ* X-ray diffraction experiments combined with microstructural observations of the recovered sample using SEM and TEM.

Experimental

In-situ X-ray diffraction experiments were carried out using sintered-diamond multi-anvil apparatus "MAX-III" installed at KEK-PF. White X-ray from synchrotron radiation was used as the incident X-ray beam and the diffracted beam was measured by the energy dispersive method. Pressure was evaluated from the equation of state of gold. The starting material is a sintered mixture of $Mg_3Al_2Si_3O_{12}$ pyrope (grain size is 3.2 μm) and gold. It was compressed to the desired pressure at room temperature, and then heated to the desired temperature at constant oil pressure. When the temperature reached to the desired value, it was kept constant and time-resolved X-ray diffraction profiles were taken every 10-200 seconds. In this way, we observed decomposition kinetics of pyrope into perovskite and corundum at 26.2-31.0 GPa and 1000-1400°C.

Results and Discussion

The post-garnet transformation occurred by grain-boundary nucleation and growth mechanisms. Perovskite and corundum grew with rectangular and granular shape, respectively, thus dissociated post-garnet assemblages do not show the lamellar texture as observed in the post-spinel assemblages [2]. This suggests that the growth requires long-range diffusion. Obtained kinetic data (Fig. 1) was analyzed based on the observed transformation mechanisms. The rate equation [3] is given by,

$$V = 1\text{-}\exp\{-2SX(t)\} \quad (1)$$

, where V is the transformed volume fraction, S is the area of the grain boundary, and $X(t)$ is the growth distance at time t. The area of grain boundary can be expressed by $3.35/d$, where d is the grain size of the parental phase. $X(t)$ is described by kt^n, where k and n are constants. The n-value was estimated to be very small and less than 1 in the post-garnet transformation, which means that the growth rate is time-dependent and significantly decreases with time contrary to the post-spinel transformation [1]. Consequently, the rate of post-garnet transformation is much slower than that of the post-spinel transformation. Differences in kinetics of these transformations might have important implications for buoyancy of the subducted oceanic crust and formation of the garnetite layer at the top of the lower mantle.

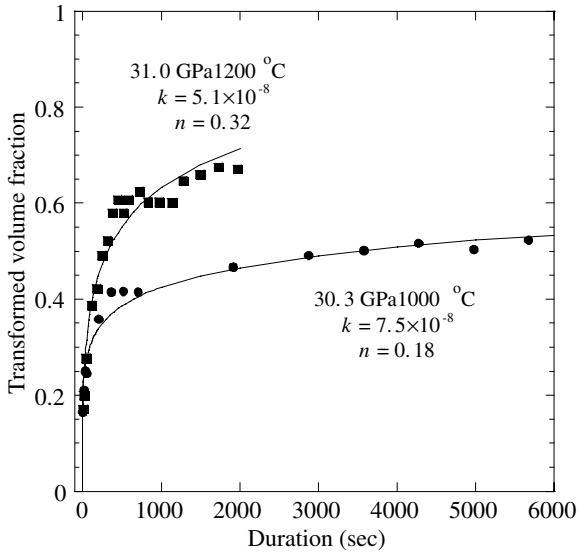

Fig. 1 Plots of transformed fraction with the heating duration at the desired temperature. Curves and kinetic parameters obtained by the least-square fits of equation (1) are also shown.

References

[1] T. Kubo et al., Phys. Earth. Planet. Inter. 129, 153 (2002).
[2] T. Kubo et al., *Geophys. Res. Lett.* 27, 807 (2000).
[3] J. W. Cahn, *Acta Metall.* 4, 449 (1956).

*tkubo@mail.cc.tohoku.ac.jp

18C/2000G220

Pressure-induced phase transition of LuSb with NaCl-type structure

Junichi HAYASHI[1], Kouji HIRANO[1], Ichimin SHIROTANI*[1] Takumi KIKEGAWA[2]
[1]Muroran Institute of Technology, Muroran 050-8585, Japan
[2] KEK-PF, Tsukuba, Ibaraki 305-0801, Japan

Introduction

Using synchrotron radiation, x-ray diffraction of LnSb(Ln = Dy, Ho, Er and Tm) has been studied up to 40 GPa at room temperature.[1,2] First-order phase transitions of LnSb with the crystallographic change occur at high pressures. The structure of the high-pressure phases of LnSb(Ln = Dy, Ho, Er and Tm) is a CsCl-type structure.

Using synchrotron radiation we have studied the x-ray diffraction of LuSb with the NaCl-type structure up to 33 GPa at room temperature. The pressure-induced phase transition for the compound is observed above 24 GPa.

Experimental

LuSb was prepared by reaction of stoichiometric amounts of each rare earth metal and antimony in a sealed silica tube at around 800 °C.

Using synchrotron radiation the powder x-ray diffraction patterns of LuSb were measured with a diamond-anvil cell and the imaging plate up to 33 GPa at room temperature. Incident beam was monochromatized by Si(111) double crystal to a wavelength of 0.6196 Å. The pressure in the diamond-cell was determined from a pressure shift in the sharp R-line fluorescence spectrum of ruby. A 4:1 methanol-ethanol solution was used as the pressure transmitting fluid.

Results and Discussion

Figure 1 shows powder x-ray diffraction patterns of LuSb at high pressures. The profile indicates only characteristic lines of the NaCl-type structure at around 0.6 GPa. The d-values of 111, 200, 220, 311, 222, 400, 420, 422, 440, 600 and 620 lines of LuSb decrease with increasing pressure up to 21 GPa. New diffraction lines appear above 24 GPa and grow with increasing pressure. Low and high-pressure phases coexist in the wide pressure range. A single phase of the new high-pressure phase is obtained above 33 GPa. When the pressure is removed, the diffraction lines of the NaCl-type structure reappear at around 12 GPa. The x-ray diffraction pattern of the high-pressure phase of LuSb can be assigned by the index of the cubic CsCl-type structure. The lattice constant of the high-pressure phase of LuSb with the CsCl-type structure is 3.46 Å at around 33 GPa.

Figure 2 shows relative unit cell volume vs. pressure curve for LuSb. The cell volume with NaCl-type structure decreases with increasing pressure up to 21 GPa. The structural change to the CsCl-type structure occurs with volume collapse of about 1 %.

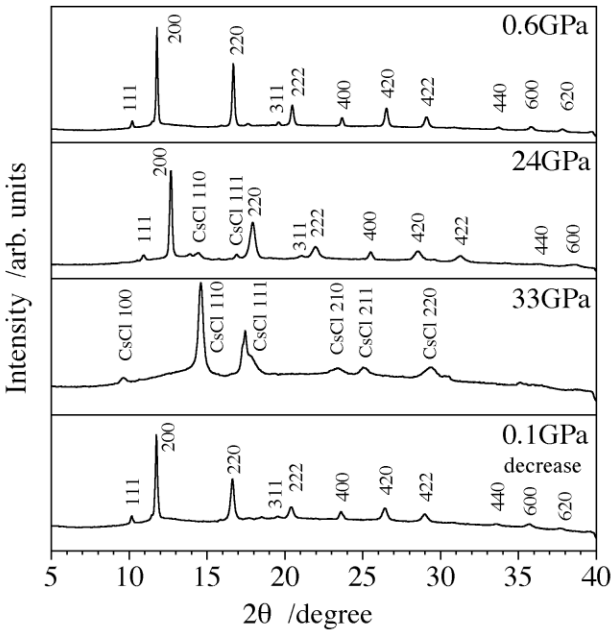

Fig. 1 Powder x-ray diffraction pattern of LuSb at high pressures.

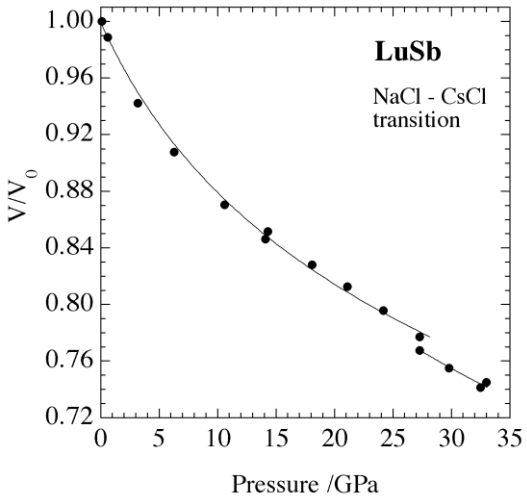

Fig. 2 Relative volume (V/V_0) - pressure curve for LuSb at room temperature.

References

[1] I. Shirotani et al., Phys. Rev. **B64**, 132101 (2001).
[2] J. Hayashi et al., Photon Factory Activity Report. **17**, 226 (1999).

* shirotani@eee.elec.muroran-it.ac.jp

10A/2001G037

Effect of pressure on the crystal structure of hydrous ringwoodite, γ-$Mg_{1.97}SiH_{0.03}O_4$

Yasuhiro KUDOH*[1], Takahiro KURIBAYASHI[1], Hiroki MIZOBATA[1], Eiji OHTANI[1], Satoshi SASAKI[2] and Masahiko TANAKA[3]
[1]Institute of Mineralogy, Petrology, and Economic Geology, Faculty of Science, Tohoku University, Sendai 980-8578, Japan
[2]Materials and Structures Laboratory, Tokyo Institute of Technology Nagatuda, Yokohama 226-8503, Japan
[3]Institute of Materials Structure Science, High Energy Accelerator Reasearch Organization, Oho, Tukuba, 305-0801, Japan

The specimen used in this study was a single crystal of hydrous ringwoodite synthesized by Ohtani and Mizobata (1998)[1] using a multi-anvil apparatus at conditions of 1680°C and 22 GPa. Electron microprobe analysis showed a chemical composition of 42.83wt% SiO_2, 56.42 wt% MgO, yielding a total wt% of 99.25 (H_2O excluded) with Mg/Si being 1.97. The H_2O content measured by SIMS was 0.2(0.004) wt %. The unit cell content is calculated to be $Mg_{1.97}SiH_{0.03}O_4$. Sets of X-ray diffraction intensities up to 7.9 GPa to $\sin\theta/\lambda$ = 0.87 $Å^{-1}$ were measured with a single crystal of 35×35×24 m using synchrotron radiation of wave lengths 0.6998 Å, 0.7017 Å, 0.6958 Å, 0.6961 Å and 0.7019 Å at ambient pressure, 3.2 GPa, 5.0 GPa, 6.2GPa and 7.9 GPa, respectively at the beam line BL-10A, Photon Factory, High Energy Accelerator Reasearch Organization, Tukuba, Japan. The wave lengths were alibrated by the unit cell constants of a ruby standard crystal. The modified Merrill-Bassett type diamond anvil pressure cell [2] was used. The 4:1 fluid mixture of methanol and ethanol was used for pressure medium and SUS301 plate was used for gasket. The pressure was calibrated using the ruby fluorescence method. The unit cell parameters obtained using 18~36 reflections with 2 from 16° to 50° are given in Table 1. The calculated isothermal bulk modulus using the unit cell volumes at ambient pressure, 3.2 GPa, 5.0 GPa, 6.2GPa and 7.9 GPa with the third-order Birch-Murnaghan equation of state assuming K'=4 was K_0=184(6) GPa and is compared with those of anhydrous ringwoodite (Table 2). The density calculated with the unit cell content $Mg_{1.97}SiH_{0.03}O_4$ and the unit cell volume at ambient pressure was 3.544 gr/cm^3. The 3.544 value is 0.5% smaller than the 3.563 gr/cm^3 value of anhydrous ringwoodite (Sasaki et al., 1982)[6]. The density and bulk modulus of hydrous ringwoodite $Mg_{1.97}SiH_{0.03}O_4$ gave 7.2 km/s bulk sound velosity of seismic wave which is equal to that of anhydrous ringwoodite, implying that hydrous ringwoodite is invisible to seismic wave. According to Weidner and Wang (2000)[7], half of the C layer of the earth's mantle is thought to be composed of ringwoodite. The 0.2 wt% of H_2O of hydrous ringwoodite imply that approximately ten times as much water can be stored in the lower part of the earth's mantle as entire ocean keeps. Analyses of crystal structures up to 7.9 GPa are in progress.

Table 1. Unit cell parameters

P(GPa)	a (Å) *	V ($Å^3$)	λ(Å)
0.0	8.065(1)	524.6(1)	0.6998
3.2	8.014(1)	514.6(3)	0.7017
5.0	7.996(2)	511.2(3)	0.6958
6.2	7.993(2)	510.6(4)	0.6961
7.9	7.962(1)	504.8(3)	0.7019

Table 2. Kulk moduli (K_0) of anhydrous and hydrous ringwoodite

H_2O(wt%)	K_0 (GPa)	K_0'	Reference
0.0	184(3)[a]		Weidner et al. (1984)[3]
0.0	184(2)	4.8[b]	Hazen (1993)[4]
0.0	182(3)	4.2(3)	Meng et al. (1994)[5]
0.2	184(6)	4[b]	This study

[a]Diabatic, [b]Fixed

References

[1] E. Ohtani, H. Mozobata, *Intern. Miner. Assoc. 17th General Meeting, Abstract*, A43 (1998)
[2] Y. Kudoh, H. Takeda, *Physica* **139&140 B**, 333 (1986)
[3] D.J. Weidner, H. Sawamoto, S. Sasaki, M. Kumazawa, J. Geophys. Res., **89**, 7852 (1984)
[4] R.M. Hazen, Science **259**, 206 (1993)
[5] Y. Meng, D.J. Weidner, G.D. Gwanmeisa, R.C. Liebermann, M.T. Vaughan, Y. Wang, K. Leinenweber, R.C. Pacalo, A. Yeganeh-Haeri, Y. Zhao, J. Geophys. Res., **98**, 22199 (1993)
[6] D.J. Weidner, Y. Wang, In S. Karato, A. Forte, R. Liebermann, G. Masters, L. Strixrude (eds), Earth's Deep Interior, 215 (2000)
[7] S. Sasaki, C.T. Prewitt, Y. Sato, E. Ito, J. Geophys. Res., **78**, 7829 (1982)

*ykudoh@mail.cc.tohoku.ac.jp

NE5C, 14C2/2001G057

High-pressure phase transitions of $Zn(OH)_2$

Keiji KUSABA*[1], Takumi KIKEGAWA[2]
[1]IMR, Tohoku Univ., Katahira 2-1-1, Aoba-ku, Sendai 980-8577
[2]KEK-PF, Tsukuba, Ibaraki 305-0801, Japan

Introduction

High-pressure and high-temperature behavior of hydroxides is very important to consider an origin and a cycle of water of the earth. There have been some investigations of $M(OH)_2$-type hydroxides under high-pressure as a simple model of general hydroxides. Almost $M(OH)_2$-type hydroxides except for $Zn(OH)_2$ and $Be(OH)_2$ have the $Cd(OH)_2$-type structure at ambient condition. $Zn(OH)_2$ and $Be(OH)_2$ have a peculiar orthorhombic structure, in which a cation is in a tetrahedral coordination site. The detail of high-pressure and high-temperature behavior of $Zn(OH)_2$ has not been observed yet, however a high-pressure phase with the $Cd(OH)_2$-type structure was reported [1].

The aims of the present study are to search new phase transitions, and to investigate the $Cd(OH)_2$-type phase in detail.

Experiment

The starting material of ε-phase with the peculiar orthorhombic structure was synthesised by an aqua-solution reaction.

In-situ X-ray observation under high-pressure and high-temperature conditions was carried out by the energy-dispersive type X-ray powder diffraction method with the MAX80 system at AR-NE5C and the MAXIII system at BL-14C2. The details of the *in-situ* observation method were described in our report [2].

Result and discussion

Figure 1 shows typical X-ray diffraction patterns of $Zn(OH)_2$. In the present study, we observe three phases except for the orthorhombic phase (Fig. 1-a), in the pressure and temperature range up to 15GPa and 400°C.

A new phase (High Pressure Phase I; HPPI) is observed in the pressure range higher than 2GPa. The X-ray diffraction pattern of the HPPI at 14.5GPa and 27°C is too broadening to be indexed (Fig. 1-b).

In the elevating-temperature process at about 14GPa, the X-ray diffraction pattern is drastically changed at 200°C. Figure 1-c) shows the X-ray diffraction pattern for the single phase of the HPPII. The crystal system has not been determined yet.

The HPPII furthermore transforms to the HPPIII in the elevating-temperature process (Fig. 1-d). The X-ray diffraction pattern of the HPPIII can be explained as the $Cd(OH)_2$-type structure. The hexagonal cell parameters of the HPPIII at 14.2GPa and 400°C are determined to be a=3.075(1)Å and c=4.318(3)Å.

The HPPIII is quenchable at ambient condition. An anisotropic behavior of the HPPIII is observed in the decompression process at room temperature; the *c*-direction is more compressive than the *a*-direction. It can be explained by a large compressibility of a van der Waals bond between layers in the $Cd(OH)_2$-type structure.

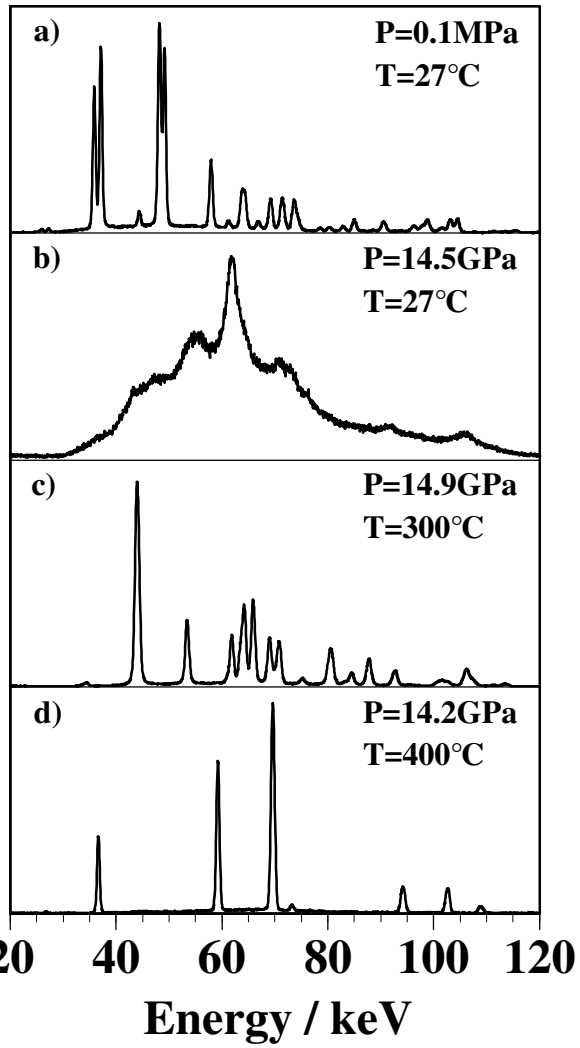

Fig. 1 X-ray diffraction patterns of Zn(OH)2 taken 2θ=4.51°. a) the ε-phase with orthorhombic structure, b) the HPPI, c) the HPP-II and d) the HPPIII with the $Cd(OH)_2$-type structure.

References

[1] Baneyeva *et al*., Geochem. Int. 6, 807 (1969).
[2] Kusaba *et al*., J. Phys. Chem. Solids 63, 651 (2002).

* kusaba@imr.tohoku.ac.jp

NE5C, 14C2/2001G227

High-pressure behavior of Si-Ge solid solution system

Keiji KUSABA*[1], Takumi KIKEGAWA[2]
[1]IMR, Tohoku Univ., Katahira 2-1-1, Aoba-ku, Sendai 980-8577, Japan
[2]KEK-PF, Tsukuba, Ibaraki 305-0801, Japan

Introduction

There have been many investigations of high-pressure behaviors of silicon and germanium. Compression behaviors of both elements were similar to each other, but decompression behaviors were very different. In the case of Si, the high-pressure phase with the β-tin type structure converted to a body-centered cubic phase (BC8-type phase) in a slow pressure-release process. In the case of Ge, a simple-tetragonal phase (ST12-type phase) was obtained. On the other hand, there are few investigations of Si-Ge solid solution system under high-pressure condition. The aim of this study is to investigate Si-Ge solid solution system in the slow pressure-release process.

Experiment

Six kinds of materials (Ge_xSi_{1-x}; x = 0.00, 0.25, 0.50, 0.75, 0.94 and 1.00) were examined in this study. The powdered material was put in an MgO capsule to protect from chemical reactions. *In-situ* X-ray observation was carried out by the energy-dispersive type X-ray powder diffraction method with MAX80 at AR-NE5C and MAXIII at BL-14C2. The details of the *in-situ* observation method were described in our report [1].

The average decompression rate was about 1GPa/hour in this study.

Result

The BC8-type phase is observed in the chemical composition between x = 0 and x = 0.75 at Ge_xSi_{1-x}, and the ST12-type phase is obtained in the cases of x = 0.94 and 1.00.

Figure 1 shows X-ray diffraction patterns of GeSi as a typical case. The diamond-β-tin type phase transition is observed (Fig. 1-a and –b). In the decompression process, the β-tin type structure reverts to the R8-type structure, which is a rhombohedral-distorted BC8 type structure (Fig. 1-c). The R8-type structure furthermore transforms to the BC8-type structure in the decompression process (Fig. 1-d). At ambient condition, the unit cell parameter of the BC8-type GeSi is a = 6.782(1)Å and the volume of the BC8-type phase is 8.42% smaller that that of the diamond-type phase.

The cubic cell parameter of the BC8-type structure *vs.* atomic ratio is plotted in Fig. 2. The present result is a typical case of "Vegard's rule".

Reference

[1] Kusaba *et al.*, J. Phys. Chem. Solids 63, 651 (2002).

* kusaba@imr.tohoku.ac.jp

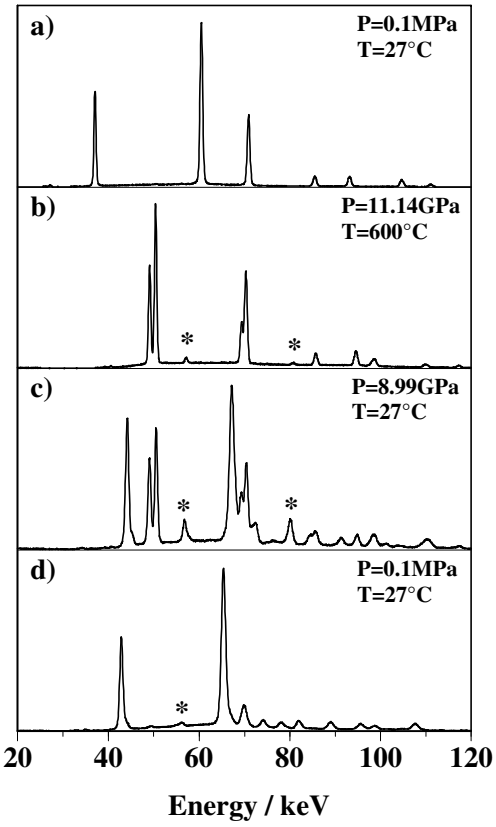

Fig. 1 Powder X-ray diffraction patterns of GeSi, taken at 2θ=600°; a) the diamond-type phase, b) the β-tin type phase, c) a mixture of the β-tin type phase and the R8-type phase and d) the BC8-type phase. Asterisk marks indicate diffraction lines from the MgO capsule.

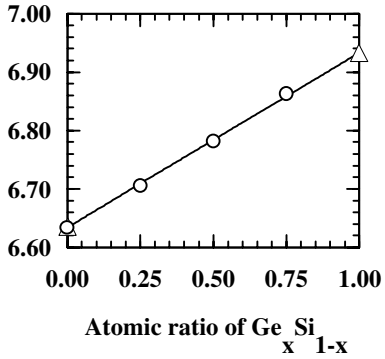

Fig. 2 The cubic cell parameters of the BC8-type phases are plotted as a function of its chemical composition. Circle and triangle marks show the resent results and previous reports, respectively

10A/2001G243

Crystal structure of humite, $Mg_7Si_3O_{12}(OH, F)_2$ at 2.7 GPa

Takahiro KURIBAYASHI[1], Yasuhiro KUDOH[1], Masahiko TANAKA[2]
[1]Graduate School of Science, Tohoku University, Sendai 980-8578 Japan
[2] KEK-PF, Tsukuba, Ibaraki 305-0801, Japan

Introduction

Humite, $Mg_7Si_3O_{12}(OH, F)_2$, belongs to humite minerals described as $n Mg_2SiO_4 \cdot Mg(OH, F)_2$ (n=1, 2, 3 and 4). Humite minerals such as chondrodite (n=2) and clinohumite (n=4) were stable under high pressure and high temperature conditions about -10 GPa, -1000ºC [1-2]. It is therefore considered that humite minerals would play an important role for the transportation and as a reservoir of water in the subduction zone. However the behaviors of humite structure under high pressure and temperature condition is little known. In this study, we report the cell parameters and the crystal structure of humite at 2.7 GPa to understand the effects of pressure on the structures of humite minerals.

Experimental Procedure

The sample used for this study is from Tilley Foster Mine, Brewster New York, U.S.A.. A single crystal of humite (50×40×30 mm in size) was mounted in a modified diamond anvil cell [3] with a small piece of ruby, which used for pressure marker. The 4:1 fluid mixture of methanol and ethanol was used for pressure medium and SUS301 plate was used for gasket. Pressure was determined by ruby fluorescence method [4]. The wavelength of synchrotron radiation (λ=0.6958 Å) is calibrated by the unit cell constants of a ruby standard crystal at ambient condition. The X-ray diffraction data were measured with an automated four-circle diffractometer at the beam line BL-10A, Photon Factory, High Energy Accelerator Research Organization. The unit cell parameters were determined from 25 centered reflections in the 2θ range between 15.6º and 30.2º. Lattice constants of humite displayed as orthorhombic symmetry within the limit of standard deviation. The X-ray reflection intensity data of humite at 2.7 GPa were collected up to $\sin\theta/\lambda<0.79$ Å^{-1} (maximum 2θ is 66.7º). The 3/8 of a reciprocal sphere was measured and a total of 2467 reflections were obtained. After background and Lorentz corrections, the symmetrically equivalent reflections were averaged by the Laue symmetry of mmm. 343 reflections ($Io > 2.0\sigma(Io)$) were used for the structure refinement of data set at 2.7 GPa. The model (space group Pbnm (No.62)) by Ribbe and Gibbs (1971) was used for the initial parameters of humite structure. Final agreements factors were R=9.4 and Rw=7.6%, applying the $1/\sigma^2(Fo)$ weight for all reflections. All calculations were performed with the teXsan crystallographic software package of Molecular Structure Corporation (1992).

Results

The unit cell parameter of humite at 2.7 GPa is a=4.715(4) Å, b=10.165(7) Å, c=20.714(4) Å and V=992.8(10) Å^3. The a/a_0, b/b_0, c/c_0 and V/V_0 ratios are 0.995, 0.991, 0.993 and 0.979. The stacking direction [100] is most stiff and the [010] direction is most compressible. This trend is the same as the other humite minerals (*ex.* the linear compressibility of each direction of chondrodite is β_a=1.88(3), β_b=2.80(3), β_c=2.79(3) ($\times 10^{-3}$/GPa), respectively (data from [5]). The predicted isothermal bulk modulus of humite is calculated as K_{0T}=117 GPa using the Birch-Murnaghan equation of state with assuming a pressure derivative K′=4. This value is consistent to the trend in humite minerals. The final atomic coordinates are given in Table 1. The mean distances of both tetrahedra (1.62(2) Å for Si1 and 1.64(2) Å for Si2) at 2.7 GPa are almost unchanged. In contrast, the mean distance of each octahedron is 2.09(3) Å for M1, 2.14(4) Å for M2, 2.08(3) Å for M3 and 2.09(3) Å for M4, respectively. Although M1-O, M2-O and M4-O mean distances are almost unchanged under this pressure, M3-O is significantly shortened.

References

[1] K. Yamamoto and S. Akimoto, *Amer. J. Sci.*, **277**, 288-312 (1977)
[2] A. Pawley, *Contrib. Mineral. Petrol.*, **138**, 284-291 (2000)
[3] Y. Kudoh and H. Takeda, Physica B, **139 & 140**, 333 (1986)
[4] G. J. Piermarnini et al., *J. Appl. Phys.*, **46**, 2774 (1975)
[5] N. L. Ross and W. A. Crichton, *Am. Mineral.*, **86**, 990-996, (2001)

Table 1. Final atomic coordinates of humite at 2.7 GPa

Site	x	y	z	Biso
M1	0.0000(23)	0.3778(13)	0.1766(4)	0.3(2)
M2	0.5143(33)	0.1521(19)	0.25	0.4(3)
M3	0.0108(20)	0.0964(12)	0.1108(4)	1.1(2)
M4	0.4930(22)	0.8644(14)	0.0278(4)	1.1(2)
Si1	0.0706(24)	0.9718(19)	0.25	0.9(3)
Si2	0.5732(14)	0.2835(12)	0.1049(4)	0.8(2)
O11	0.7356(52)	0.9580(42)	0.0366(12)	1.9(8)
O12	0.2855(72)	0.3139(60)	0.25	1.4(10)
O13	0.2192(49)	0.0281(46)	0.1873(11)	1.0(8)
O21	0.2310(41)	0.2713(45)	0.1048(13)	1.4(7)
O22	0.7794(30)	0.9259(28)	0.1081(9)	0.7(4)
O23	0.7321(35)	0.2064(50)	0.1698(10)	1.7(5)
O24	0.7250(35)	0.2069(33)	0.0470(9)	0.8(4)
OH	0.2698(43)	0.0289(42)	0.0366(12)	0.6(5)

* t-kuri@mail.cc.tohoku.ac.jp